Structural Roles of the Highly Conserved Glu Residue in the Heme Distal Site of Peroxidases†

Motomasa Tanaka, Koichiro Ishimori, and Isao Morishima*

Department of Molecular Engineering, Graduate School of Engineering, Kyoto University, Kyoto 606-01, Japan

Received October 13, 1997; Revised Manuscript Received December 1, 1997

ABSTRACT: One of the highly conserved amino acid residues in the heme distal site of various fungal and plant peroxidases, glutamic acid 64 (Glu64) in horseradish peroxidase (HRP), interacts with a distal calcium ion through a hydrogen bond with a water molecule and its peptide carbonyl oxygen on the main-chain forms the hydrogen bond network to the distal His via the adjacent Asn residue, suggesting that the Glu residue is related to the stabilization of the calcium ion and catalytic activity of peroxidase [Nagano, S., Tanaka, M., Ishimori, K., Watanabe, Y., and Morishima, I. (1996) *Biochemistry 35*, 14251−14258]. To perturb the hydrogen bond with the adjacent Asn, we replaced the Glu with Pro (E64P) or Gly (E64G), which would alter the configuration of the main chain at position 64. Both of the mutants exhibited substantially depressed oxidation activities for hydroquinone and elementary reaction rates in the catalytic cycle. However, the E64S (Glu64 → Ser) mutant, in which the configuration of the main chain and the hydrogen bond with Asn70 would not be affected but the interactions with the calcium ion are seriously perturbed by removal of the carboxylate, also showed quite low catalytic activity as observed for the E64P and E64G mutants. Spectral features for the E64S mutant are similar to those of the other mutants: the reorientation of the distal His, disruption of the hydrogen bond between the distal His and Asn70, and loss of the calcium ion. Thus, we can conclude that, in addition to forming the hydrogen bond network in the distal site, the Glu residue is a key residue for stable binding of the calcium ion, which maintains the structural integrity of the distal cavity, resulting in high peroxidase activity.

Peroxidases are a group of heme-containing enzymes that catalyze the reduction of peroxides at the expense of electrons donated by a wide variety of organic and inorganic reductants. One of the most intensively studied members of this enzyme superfamily is horseradish peroxidase (HRP). Upon addition of hydrogen peroxide, the resting ferric HRP undergoes a two-electron oxidation to yield an intermediate termed compound I. The iron of the HRP compound I is in the ferryl state and is magnetically coupled to the porphyrin π cation radical (*1*). Compound I reverts to the resting enzyme via two sequential one-electron reactions with reducing substrates. The first reaction yields a second intermediate, compound II, an oxyferryl heme without a free radical. Another one-electron reduction by a second reducing substrate completes the catalytic cycle by converting compound II to the resting state.

Although the X-ray crystal structure of HRP has not been published yet, the heme environmental architecture of HRP has been considered to be shared with that of peanut peroxidase (PnP) (Figure 1) (*2*), since both of them belong to the same class of peroxidase. Among several amino acids in the active site, a key catalytic residue is the distal histidine (distal His). On the basis of the X-ray crystal structure of cytochrome *c* peroxidase (C*c*P), Poulos and Kraut (*3*) proposed that a major role of the distal His is as a general acid−base catalyst in the formation of compound I. Experimental support for this catalytic role has recently come from the site-directed mutagenesis of C*c*P and HRP. The replacements of the distal His by Leu in C*c*P (*4*, *5*) and by Ala, Val (*6*), or Leu (*7*) in HRP gave a pronounced effect on the rate of compound I formation, the apparent bimolecular rate constant being decreased by 5−6 orders of magnitude. The catalytic activities of these mutants were suppressed due to the deceleration of the reaction rate with H_2O_2, demonstrating that the distal His is the most essential amino acid residue for peroxidase activity.

As shown in Figure 1, the distal His hydrogen-bonds with the adjacent Asn, which is highly conserved in various fungal and plant peroxidases (*2*, *8*−*14*). We have recently found that replacement of Asn70 in HRP with Val (N70V) or Asp (N70D) substantially depressed the catalytic activity to less than 10% of that of the native enzyme (*15*, *16*). The decrease of the peroxidase activity was concluded to be ascribed to less basicity and reorientation of the distal His, indicating that the His−Asn hydrogen bond improves the catalytic activity by controlling the basicity and orientation of the distal His (*16*−*18*).

† This work was supported by grants-in-aid for scientific research on priority areas "Molecular Biometallics" (08249102 to I.M.) from the Ministry of Education, Science, Culture and Sports.

* To whom correspondence should be addressed: (phone) +81-75-753-5921; (fax) +81-75-751-7611; (e-mail) morisima@mds.moleng.kyoto-u.ac.jp.

[1] Abbreviations: HRP, horseradish peroxidase isozyme C; native HRP, peroxidase isolated from horseradish isoenzyme C; wild-type HRP, recombinant horseradish peroxidase isozyme C expressed in *Escherichia coli*; PnP, peanut peroxidase; C*c*P, cytochrome *c* peroxidase; MnP, manganese peroxidase; ARP, *Arthromyces ramosus* peroxidase; ABTS, 2,2′-azidobis(3-ethylbenzothiazoline-6-sulfonic acid) diammonium salt; ICP, inductively coupled plasma.

S0006-2960(97)02527-0 CCC: $15.00
Published on Web 02/04/1998

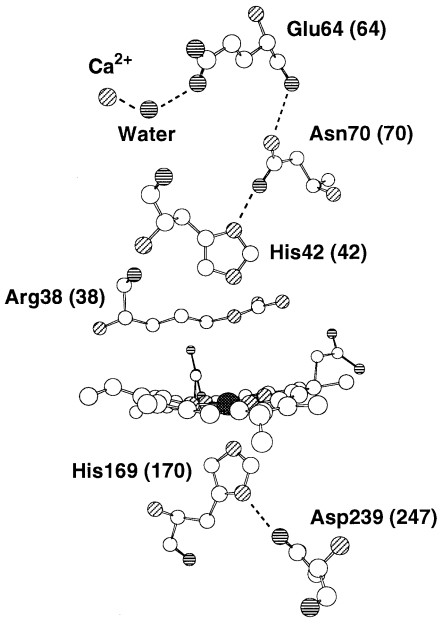

FIGURE 1: Heme environmental architecture of PnP. Amino acid numbering is for PnP, and the numbers in parentheses denote the numbering for HRP. Some key hydrogen bonds in the crystal structure are shown as dashed lines.

In the previous study, Asp70 in the N70D mutant did not form a hydrogen bond with the distal His as did Val70 in the N70V mutant, although the Asp residue has a carboxyl group that can make a hydrogen bond with $N_\delta H$ of the distal His. It should be noted here that, in the X-ray crystal structure of PnP (*2*), Asn70 in HRP forms hydrogen bonds not only with the $N_\delta H$ of the distal His but also with the peptide carbonyl oxygen of Glu64 (Figure 1), which is also highly conserved in peroxidases (*2, 8*−*14*). Therefore, it is most plausible that Asn70 is fixed at the optimal position for the hydrogen bond with the distal His by the Glu64−Asn70 hydrogen bond in peroxidases. In the N70D mutant, the hydrogen bond between Asp70 and Glu64 would be disrupted due to the amino acid substitution at position 70 and the large perturbation of the Glu64−Asp70 interactions would cause the positional change of Asp70, resulting in the breakage of the His−Asp hydrogen bond. Together with the catalytic and structural alterations in the N70D mutant, we have proposed that Glu64 is one of the crucial amino acid residues to improve peroxidase activity by controlling the basicity and orientation of the distal His through the Glu64−Asn70−His42 hydrogen bond network in the heme distal site (*16, 18*).

In addition to forming the hydrogen bond with the amino group in Asn70, the carboxylate in the side chain of Glu64 interacts with a distal calcium ion through hydrogen bonds mediated with a water molecule (Figure 1). The distal calcium ion in HRP is closely implicated with stabilization of protein structure and oxidation activity, since apoHRP is not properly refolded in the absence of the calcium ions (*19*) and removal of the bound calcium ions from native HRP results in a large decrease in peroxidase activity and thermal stability (*20*−*23*). These observations imply that the Glu residue controls the catalytic activity by stabilizing the distal calcium ion as well as by forming the hydrogen network in the heme distal site.

In the present study, we have prepared three HRP mutants in order to elucidate the catalytic and structural roles of the Glu residue. Glu64 in HRP was substituted for Pro (E64P) and Gly (E64G) to perturb the configuration of the main chain at position 64, which is expected to alter the position of the peptide carbonyl oxygen of the Glu residue hydrogen-bonded to Asn70. We also introduced a Ser residue into the Glu64 position, in which the configuration of the main chain and the hydrogen bond with Asn70 would not be affected, but the interactions with the distal calcium ion are seriously perturbed as is for the E64P and E64G mutants. The catalytic activities and structural properties of the Glu64 mutants were examined by utilizing various spectroscopies including CD, ^{1}H NMR, resonance Raman, and ICP emission.

EXPERIMENTAL SECTION

Expression and Purification of Recombinant HRPs. Site-directed mutagenesis was performed by using the T7 HRP expression vector constructed by Nagano et al. (*15*). Double-stranded DNA sequence analysis with a 373 DNA sequencer (Applied Biosystems) verified introduction of the mutation without additional mutations in the whole HRP-coding gene.

The wild-type and mutant HRPs were expressed in *Escherichia coli* (BL21 strain), and apoHRP was extracted from the inclusion bodies as reported previously (*16*). Heme reactivation of apoHRP in the presence of calcium ion and purification of holoHRP were described elsewhere (*16*). RZ values of the purified wild-type and mutant HRPs were about 3.2 and 2.8, respectively. Peroxidase concentration was estimated by the pyridine hemochrome form at the Soret band (*24*). The extinction coefficients were 103, 94, 96, and 95 $mM^{-1}\cdot cm^{-1}$ for wild-type, E64P, E64G, and E64S mutant HRPs, respectively.

Circular Dichroism (CD) Spectroscopy. CD spectra of HRPs were acquired on a Jasco J-720 CD spectrometer at ambient temperature. Mean residue α-helical contents (f_H) were evaluated from the mean residue ellipticity at 222 nm by eq 1 (*25*). CD spectra reported in this paper were an

$$f_H = -([\theta]_{222} + 2340)/30300 \quad (1)$$

average of eight scans recorded at a speed of 100 nm/min and a resolution of 0.2 nm.

Proton Nuclear Magnetic Resonance (^{1}H NMR) Spectroscopy. ^{1}H NMR measurement was performed on a Bruker Avance DRX500 spectrometer. All of the ^{1}H NMR spectra of ferric- and cyanide-ligated HRPs were recorded at 17.0 °C. Concentration of the samples for the ^{1}H NMR measurements was ∼0.5 mM in 90% H_2O or 100% ^2H_2O containing 50 mM sodium phosphate buffer, pH(D) 7.0. The pH for the enzyme solution was measured with a Beckman model 3550 pH meter. The pD value was adjusted by using 10 N NaOD and was not corrected for the isotope effect. Peak shifts were referenced to the residual water signal, which is calibrated against tetramethylsilane (TMS).

Resonance Raman Spectroscopy. Resonance Raman spectra of HRPs were recorded with excitation from a Kr^+ ion laser (Spectra Physics, model 2016) using the 406.7-nm line and from a He/Cd laser (Kinmon Electrics, model CD 1805B) using the 441.6-nm line. The resonance Raman scattering was detected with a charge-coupled device (CCD) (PAR 1530-CUV) attached to a single monochromator (Ritsu Oyo Kogaku, DG-1000). The spectral slit width was ∼150 μm. Sample solutions in a spinning quartz cell were cooled

by flushing cold nitrogen gas. The frequency calibration was performed with indene (600−900 cm^{-1}) or carbon tetrachloride (200−400 cm^{-1}) as a standard. Wild-type and mutant compounds II were prepared by adding a slight excess of H_2O_2 to the ferric solutions. Buffer systems used here were sodium phosphate buffer at pD 7.0 and borate buffer at pD 10.0. $H_2{}^{18}O_2$ was prepared from $^{18}O_2$ as described by Sawaki and Foote (*26*). Ferrous HRPs were prepared by adding a small volume of a freshly saturated sodium dithionite solution to degassed ferric solutions.

Determination of Calcium Concentration. Calcium ion in HRPs was quantified by ICP emission spectroscopy (Thermo Jarrell Ash ICAP-500, Franklin, MA). A ∼15 μM HRP solution was utilized to analyze the amount of calcium ion. The concentration of HRP was determined by the absorbance at the Soret band in the UV−visible spectrum.

Reaction with H_2O_2. Wild-type and mutant HRP compounds I were generated by adding a small excess of H_2O_2 to the ferric enzyme solution. Turnover of the ferric enzyme was monitored at various time points on a Shimadzu UV-2200 spectrophotometer at 20 °C.

Peroxidase Activities. For hydroquinone oxidation, HRP was added to a solution containing 50 μM H_2O_2 and 5−200 μM hydroquinone in 50 mM sodium phosphate buffer, pH 7.0 and the final concentration of HRPs was 5 nM. To determine the oxidation rate, the absorbance at 250 nm was monitored on a Shimadzu UV-2200 spectrophotometer at 25 °C. For 2,2′-azidobis(3-ethylbenzothiazoline-6-sulfonic acid-)diammonium salt (ABTS) oxidation, the HRP sample was added to a solution containing 1.0 mM H_2O_2 and 25−900 μM ABTS in 50 mM sodium phosphate buffer, pH 6.0, to a final concentration of 1 nM. The initial oxidation rate was determined by following the increase of the absorbance at 405 nm at 25 °C. The oxidation rates were expressed as micromolar per minute by using molar absorption coefficients of the oxidation products of hydroquinone (8.28 $mM^{-1}\cdot cm^{-1}$) (*27*) and ABTS (36.8 $mM^{-1}\cdot cm^{-1}$) (*28*). Kinetic parameters, K_m and V_{max}, were obtained from the initial oxidation rates, k_{int}, and concentration of substrate, [S] (eq 2).

$$k_{int} = (V_{max}[S])/(K_m + [S]) \quad (2)$$

Elementary Reaction Rates in the Catalytic Cycle. Formation and reduction of compound I, and reduction of compound II under pseudo-first-order condition, were monitored on a stopped-flow spectrophotometer (Unisoku) at 25 °C in 50 mM sodium phosphate buffer, pH 7.0. More than a 10-fold excess of H_2O_2 or guaiacol relative to the HRP concentration (2 μM) was utilized to ensure pseudo-first-order kinetics. The elementary reaction rates of k_1, k_2, and k_3 were determined by the absorbance change at 395, 412, and 424 nm, respectively.

Redox Potential of Fe^{2+}/Fe^{3+} Couple. The redox potentials of HRPs were monitored with platinum electrode on a Perkin-Elmer Lambda 19 UV−visible spectrophotometer. The photoreduction of the ferric HRPs was performed as previously reported (*18*). The midpoint potential (E_0) of HRP was estimated from a plot of E_h against the logarithm of percentage reduction of HRP using eq 3 (*29*). In the equation, ν and F denote the number of electrons involved in the redox reaction and the Faraday constant, respectively. The midpoint potential of HRP was corrected by utilizing phenosafranine (−252 mV) as a standard (*30*).

$$E_h = E_0 + (RT/\nu F)\ln\{[\text{oxidized HRP}]/[\text{reduced HRP}]\} \quad (3)$$

Table 1: Mean Residue Molar Ellipticities at 222 nm and Estimated α-helical Contents of Wild-Type, E64P, E64G, and E64S HRPs in Resting States

HRP	$-[\theta]_{222} \times 10^{-4}$ [a]	α-helix (%)
wild-type	1.45	40
E64P	1.48	41
E64G	1.42	39
E64S	1.52	42

[a] Mean residue ellipticity in deg·cm^2·$dmol^{-1}$.

RESULTS

CD Spectroscopy. A CD spectrum in the far-UV region provides us with information about the secondary structures in a protein (*31*). The α-helical content can be estimated by using the molar ellipticity at 222 nm (eq 1) (*25*). All of the mutants exhibited similar spectral patterns, which were indistinguishable from that of wild-type HRP (data not shown). Table 1 collects the α-helical contents of the HRPs calculated from eq 1. The α-helical contents of the mutants were in good agreement with that of the parent enzyme. This result together with the similarity of the UV−visible absorption spectra between the mutant and wild-type HRPs (data not shown) suggests that all of the mutants were properly refolded as was the wild-type enzyme.

^{1}H NMR Spectroscopy. We utilized ^{1}H NMR spectroscopy to investigate heme environmental structures of HRPs. Figure 2 displays hyperfine-shifted ^{1}H NMR spectra of the resting states for the wild-type and mutant enzymes in 90% H_2O/10% ^2H_2O at 17.0 °C. For the wild-type enzyme, four peaks, which have been assigned to the heme peripheral methyl groups, were observed at 84, 76, 72, and 56 ppm (5-, 1-, 8-, and 3-methyl groups) (*32*, *33*). It is noteworthy that all the ferric mutants exhibited similar spectral features and their hyperfine-shifted resonances from the methyl groups of the porphyrin ring appeared at 82, 80, 69, and 58 ppm (Figure 2). Although the resonance positions of the signals were slightly shifted, the average position of the four methyl resonances (72 ppm for the wild-type enzyme) was not changed by the mutation (72 ppm for the Glu64 mutants), suggesting that the geometry of the heme is almost similar (*34*). A small resonance at 101 ppm for wild-type HRP, which has been assigned to $N_\delta H$ of the proximal His (His 170) (*32*, *33*), was also found at the same position for the mutant enzymes. The coordination structure of the proximal His to the heme iron was not perturbed.

To gain further insight into the heme environmental structure, we measured the ^{1}H NMR spectra of cyanide-ligated HRPs. Figure 3 depicts the hyperfine-shifted region of the cyanide-ligated wild-type and Glu64 mutant HRPs in 90% H_2O/10% ^2H_2O at 17.0 °C. As shown in this figure, the amino acid substitution at Glu64 induced some significant spectral changes, while all the mutants examined here showed an almost identical spectral pattern. Although the signal assignments have not yet been done due to the limited amount of the mutant proteins, the high similarity of the NMR spectra between the Glu64 mutants and our previous

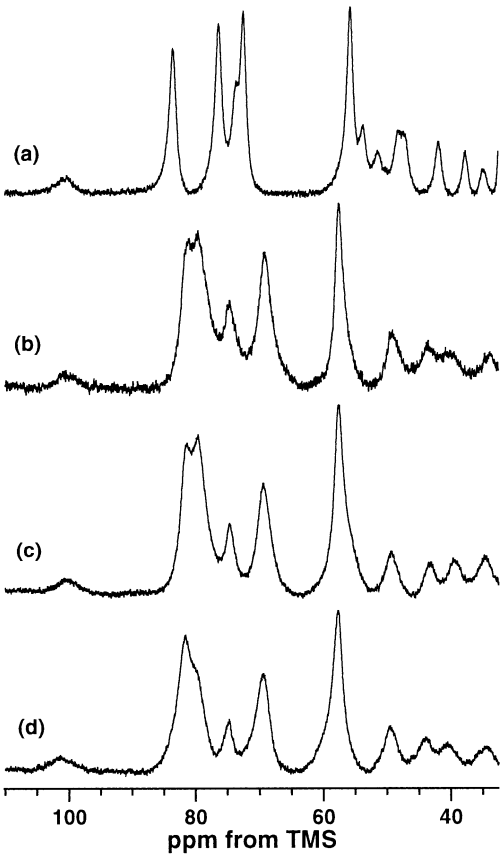

FIGURE 2: ^{1}H NMR spectra in the hyperfine-shifted region of resting states of (a) wild-type, (b) E64P, (c) E64G, and (d) E64S HRPs in 90% H_2O/10% ^2H_2O buffer, pH 7.0 at 17.0 °C.

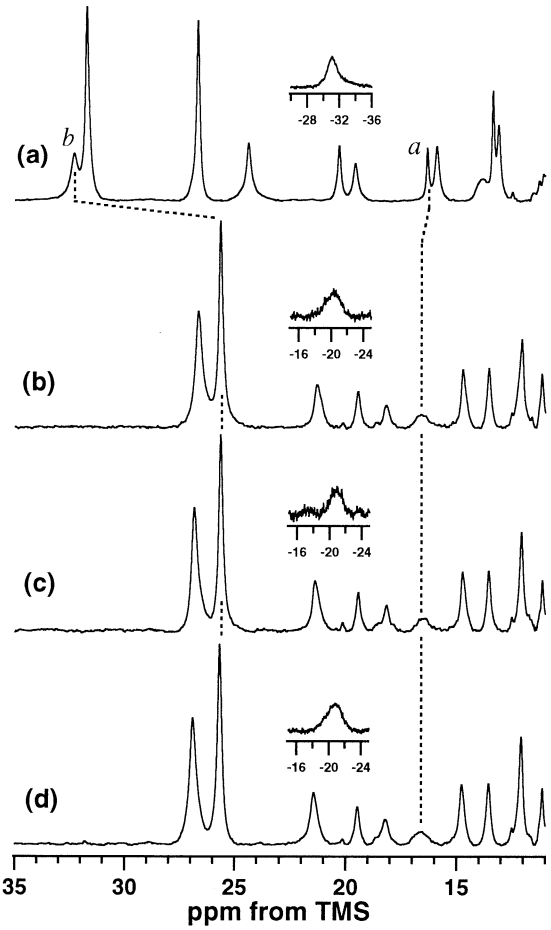

FIGURE 3: ^{1}H NMR spectra in the hyperfine-shifted region of cyanide-ligated (a) wild-type, (b) E64P, (c) E64G, and (d) E64S HRPs in 90% H_2O/10% ^2H_2O buffer, pH 7.0 at 17.0 °C. The signals *a* snd *b* are assigned to $N_\delta H$ and $N_\epsilon H$ of the distal His, respectively

mutant, N70D, allowed us to assign some NMR signals to the heme peripheral groups and amino acid residues near heme iron. In the N70D mutant, the isotope and NOE effects on the hyperfine-shifted NMR signals were utilized to assign the resonances (*18*). A broad signal at 16.6 ppm in the spectra of the Glu64 mutants disappeared in the deuterated buffer (Figure 4), which corresponds to $N_\delta H$ of the distal His in the N70D mutant (*18*). The peak intensity of a signal at 25.7 ppm (3-methyl group) in the spectra of the mutants was notably decreased in the deuterated buffer (Figure 4),[2] suggesting that a resonance derived from $N_\epsilon H$ of the distal His was superimposed, which was also encountered for the N70D mutant (*18*). The $N_\epsilon H$ resonance of the distal His in the mutants exhibited an upfield shift of 6 ppm. In the high-field region, a broadened signal of the proximal His $C_\epsilon H$ in the mutants experienced a prominent large downfield shift from −31.1 (wild type) to −20.9 ppm with the amino acid substitution (Figure 3). In addition, two resonances at −5.9 and −7.2 ppm, which have been assigned to $C_\beta H$ and $C_\delta H$ of the distal arginine (Arg38) (*35*), were not detected in the mutants, probably due to the downfield shift to the unresolvable region of the NMR spectra (data not shown). Such prominent changes in the NMR signal were observed not only for the resonances from the amino acid residues near the heme iron but also for those from the heme peripheral group. The 8-methyl resonance experienced a large upfield shift with the mutation. Assignments for the specific resonances[3] of the mutant enzymes are compiled in Table 2.

Resonance Raman Spectroscopy. Figure 5 shows resonance Raman spectra of wild-type and mutant compounds II with 406.7-nm excitation. The spectra were acquired by using ^2H_2O buffer to enhance the intensity of the Fe(IV)═O Raman band, as reported previously (*37*). The Raman band at 775 cm^{-1} in the spectrum of the wild-type enzyme has been attributed to the Fe^{IV}═O stretching vibration mode of compound II (*37*). Though the corresponding stretching mode was obscure in the mutants, the difference spectra (Figure 5C) clearly showed that the mutation induced an upfrequency shift of the Fe(IV)═O Raman band from 775 (wild type) to 782 cm^{-1} (mutants). The Raman shifts of the mutants at pD 7.0 were identical with that of the wild-type enzyme at pD 10.0 (782 cm^{-1}). Since the hydrogen bond between the ferryl oxygen and the distal Arg[4] (*38*) is disrupted in the high-pH region in the wild-type enzyme (*37*),

[2] The integrated value of the peak at 25.7 ppm relative to that at 26.8 ppm in the Glu64 mutants was decreased by ∼16% in the deuterated buffer.

[3] In the ^{1}H NMR spectrum of a cytochrome *c* peroxidase (C*c*P) N82D-CN mutant, one deuterium-sensitive resonance in the low-field region was assigned to the distal Arg (*36*). However, resonances from the distal Arg were not observed in the low-field region of the ^{1}H NMR spectrum of HRP-CN (*35*).

[4] Although the distal Arg forms the hydrogen bond with the ferryl oxygen in C*c*P compound I (*38*), the pK_a value of the acid−base transition for HRP compound II (8.5 for HRP C and 6.9 for HRP A1) would be in favor of the distal His as the hydrogen bond partner with the ferryl oxygen (*37*, *39*, *40*).

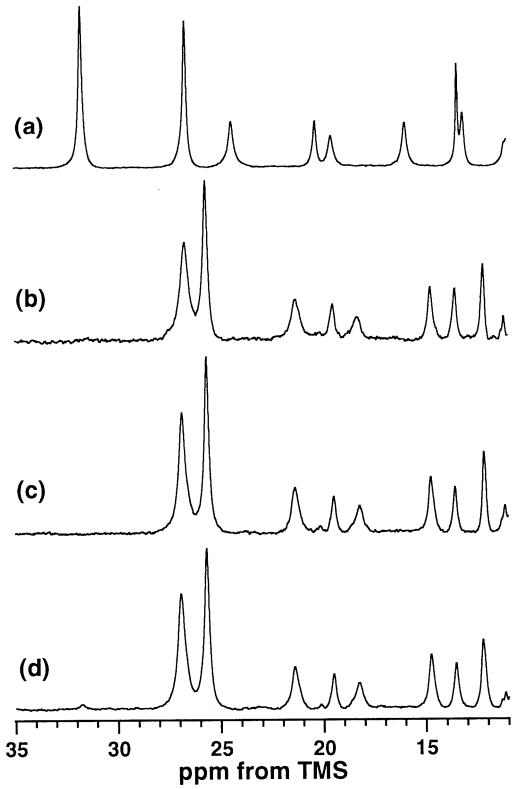

FIGURE 4: ^{1}H NMR spectra in the hyperfine-shifted region of cyanide-ligated (a) wild-type, (b) E64P, (c) E64G, and (d) E64S HRPs in 99% ^2H_2O buffer, pH 7.0 at 17.0 °C.

Table 2: Chemical Shifts (ppm) and Assignments of Heme and Amino Acid Protons of Cyanide-Ligated Wild-Type, E64P, E64G, and E64S HRPs at 17.0 °C

assignment	wild type	E64P	E64G	E64S	N70D[a]
heme 8-CH_3	31.0	26.7	26.8	26.9	27.2
heme 3-CH_3	26.2	25.7	25.7	25.7	25.5
His170 $C_\epsilon H$	−31.1	−20.4	−20.9	−20.9	−18.2
His42 $N_\epsilon H$	31.8	25.7	25.7	25.7	25.5
His42 $N_\delta H$	16.4	16.6	16.6	16.6	16.7
His42 $C_\epsilon H$	13.3	12.1	12.1	12.1	13.1

[a] Measurement was performed at 23.0 °C (*18*).

the hydrogen bond is not formed at neutral pH in the Glu64 mutants. Such a higher wavenumber shift was also reported for the HRP Asn70 mutants (*17*), in which the hydrogen bond was missing at neutral pH.

Figure 6 displays resonance Raman spectra in the low-frequency region of ferrous HRPs with 441.6-nm excitation. The spectra of the reduced wild-type enzyme is characterized by a strong band at 242 cm^{-1}, which has been attributed to the stretching mode between the ferrous iron and the anionic proximal imidazole (His 170) (*41*). For the Glu64 mutants, the Fe^{II}−His stretching Raman band exhibited a subtle downfrequency shift to 239 cm^{-1}, indicating that the Fe^{II}−His bond is slightly weakened, presumably because the proximal His has less anionic character. However, the Fe−N_ϵ vibration frequency in the mutants was still much higher than that of myoglobin with a neutral His ligand (220 cm^{-1}) (*42*).

Determination of Calcium Concentration. Table 3 summarizes the calcium ion contents in HRPs determined by ICP emission spectroscopy. The wild-type HRP contained two calcium ions, as suggested by the X-ray crystal structure of PnP (*2*). In sharp contrast to the wild-type enzyme, the ICP emission experiment showed that only one calcium ion binds to one molecule of the Glu64 mutants.

Reaction with H_2O_2. As shown in Figure 7a, resting wild-type HRP reacts with a small excess of H_2O_2, decreasing absorbance of the Soret band, which is characteristic of compound I. In the absence of reductants, compound I was gradually reduced to compound II with a shift of the Soret peak from 402 to 420 nm and finally reverted to the resting state. Compound I of the E64P mutant was also generated and underwent reductions as depicted in Figure 7b. However, compound I of the mutant was easily reduced back to the resting state (λ_{max} = 404 nm) via compound II (λ_{max} = 420 nm), relative to that of the wild-type HRP. The time courses for the E64G and E64S mutants were quite similar to that of the E64P mutant.

Peroxidase Activities. We examined the peroxidase activity of the mutants by use of two typical substrates, hydroquinone and ABTS. Hydroquinone donates both a proton and an electron to the enzyme, whereas ABTS is only an electron donor (*16*). The kinetic parameters for the reaction with hydroquinone and ABTS under steady-state conditions are summarized in Table 4. The consequences of introducing the mutation at position 64 are dramatic. Upon oxidation of hydroquinone, V_{max} values for all the mutants decreased by a factor of 20 for the mutants, compared with those of wild-type HRP. The apparent K_m values for the oxidation of hydroquinone were also reduced by the mutation. For ABTS oxidation, however, V_{max} values were significantly increased relative to those of the parent enzyme. The mutation decreased apparent K_m values for the oxidation of ABTS ∼8-fold.

Elementary Reaction Rates. To clarify the effects of the mutation on the individual steps of the peroxidase cycle, the elementary reaction rates were examined with a stopped-flow spectrophotometer. The elementary reaction rates for the mutant and parent enzymes are listed in Table 5. The formation rate of compound I (k_1) for wild-type HRP (1.3×10^7 $M^{-1}\cdot s^{-1}$) is in accord with the value (1.4×10^7 $M^{-1}\cdot s^{-1}$) reported by Smith et al. (*28*). The replacement of Glu64 severely depressed the k_1 value for all the mutants.

The reduction rate of compound I (k_2) was determined by using guaiacol as a reductant. The k_2 value for wild-type enzyme (5.3×10^6 $M^{-1}\cdot s^{-1}$) is virtually the same as the value reported by our group (6.2×10^6 $M^{-1}\cdot s^{-1}$) (*16*) and Yamazaki and Yokota (*43*) (9×10^6 $M^{-1}\cdot s^{-1}$). The Glu64 mutants exhibited ∼5-fold reduced k_2 values (Table 5).

By using guaiacol as a reductant, the reduction rates of compound II (k_3)[5] were obtained. The k_3 value of the wild-type HRP (3.6×10^5 $M^{-1}\cdot s^{-1}$) was identical to the value previously reported (3×10^5 $M^{-1}\cdot s^{-1}$) (*43*), whereas the mutations moderately depressed the k_3 values by 50%.

Redox Potential of the Fe^{2+}/Fe^{3+} Couple. The potentiometric titration curve for the Fe^{2+}/Fe^{3+} couple by eq 3 conformed to a one-electron oxidation−reduction equilibrium with a midpoint potential compiled in Table 6. The value

[5] It should be noted that saturation kinetics is sometimes observed in the reaction rate of compound II to resting state, which makes it difficult to estimate the exact reaction rates (*44*). In the present study, the k_3 value was obtained as the second-order rate constant from the linear part of the rate vs [guaiacol] profile.

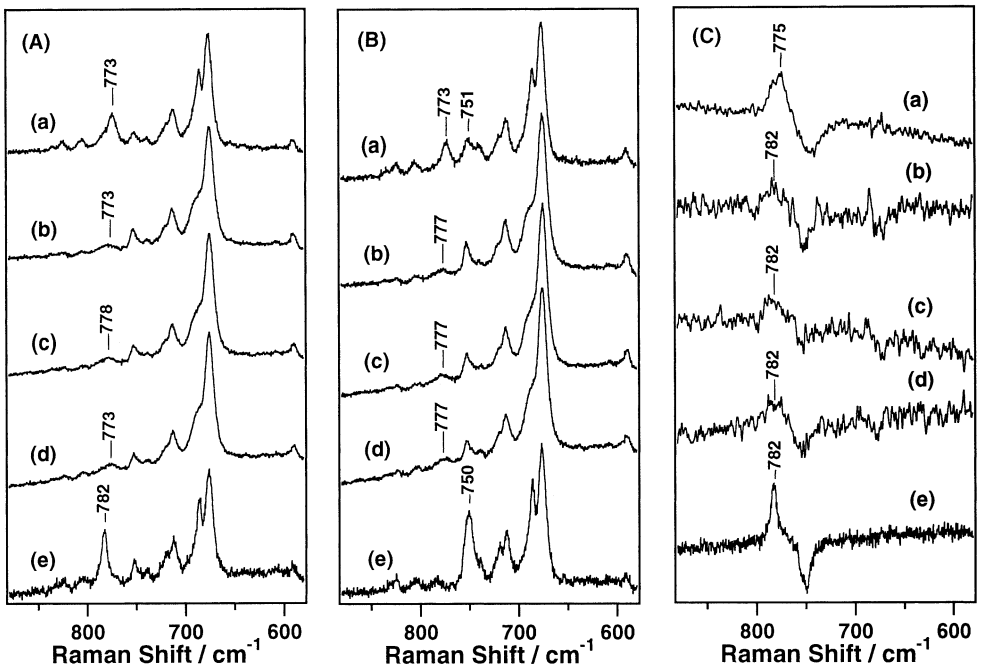

FIGURE 5: Resonance Raman spectra of compounds II of (a) wild-type, (b) E64P, (c) E64G, and (d) E64S HRPs at pD 7.0 and (e) wild-type HRP, at pD 10.0 by 406.7-nm excitation. Laser power, 4.5 mW; accumulation time, 8 min; enzyme concentration, 30 μM. Key: Compound II derived from (A) $H_2{}^{16}O_2$ and (B) $H_2{}^{18}O_2$ (C) $H_2{}^{16}O_2 - H_2{}^{18}O_2$.

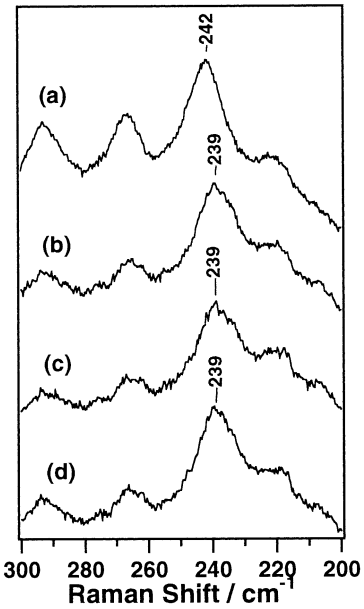

FIGURE 6: Resonance Raman spectra of ferrous states of (a) wild-type, (b) E64P, (c) E64G, and (d) E64S HRPs at pH 7.0 by 441.6-nm excitation. Laser power, 15 mW; accumulation time, 4 min; enzyme concentration, 30 μM.

Table 3: Calcium Contents of Wild-Type, E64P, E64G, and E64S HRPs

HRP	mol of Ca^{2+}/mol of HRP
wild-type	2.1 ± 0.1
E64P	1.1 ± 0.1
E64G	1.1 ± 0.1
E64S	1.0 ± 0.1

of −261 mV for wild-type enzyme coincides well with the value (−258 mV) for native HRP reported by Yamada et al. (*29*), whereas the midpoint potentials for all the three mutants increased by ∼60 mV.

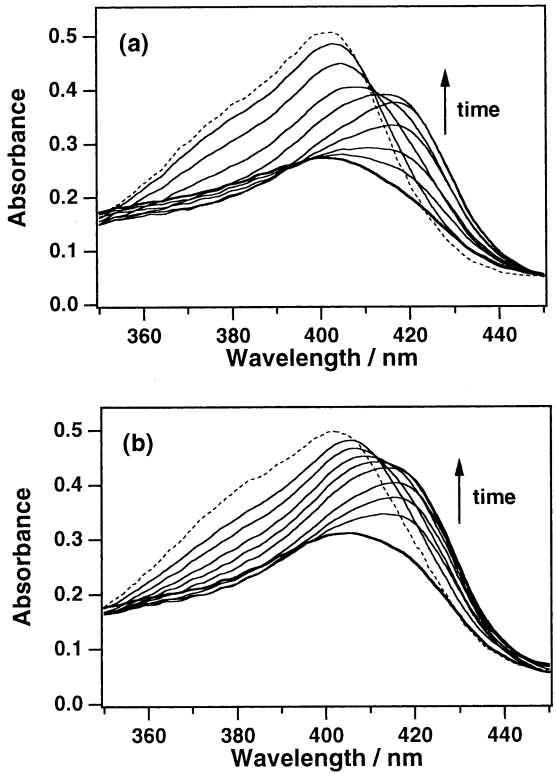

FIGURE 7: Time-dependent UV−visible absorption spectral changes of (a) wild-type and (b) E64P HRPs after the addition of a small excess of H_2O_2. The dotted line shows the spectrum before the addition of H_2O_2. The repetitive scans were recorded at (a) 0 (thick line), 1, 5, 20, 50, 110, 170, 290, and 470 min and (b) 0 (thick line), 1, 2, 3, 6, 9, 13, 21, and 54 min after the addition of H_2O_2.

DISCUSSION

Heme Environmental Structure. Although overall structures of the mutants were similar to wild-type HRP as shown by CD spectroscopy, structural changes in the distal site were

Table 4: Kinetic Parameters of Oxidation for Hydroquinone and ABTS by Wild-Type, E64P, E64G, and E64S HRPs

	hydroquinone		ABTS	
HRP	K_m (μM)	V_{max} (μM·min^{-1})	K_m (μM)	V_{max} (μM·min^{-1})
wild-type	36 ± 3	309 ± 21	255 ± 12	9.7 ± 0.6
E64P	17 ± 2	12 ± 3	31 ± 2	28 ± 2
E64G	17 ± 1	13 ± 2	30 ± 3	29 ± 4
E64S	15 ± 2	14 ± 2	31 ± 2	24 ± 2
wild-type[a]	37	281	286[b]	71[b]
N70V[a]	19	18	279[b]	217[b]
N70D[a]	33	29	278[b]	234[b]

[a] Reference 16. [b] Concentration of HRP (0.5 nM) is different from that in this study (1 nM).

Table 5: Elementary Reaction Rates (M^{-1}·s^{-1}) of Wild-Type, E64P, E64G, and E64S HRPs

HRP	$k_1/10^7$	$k_2/10^6$	$k_3/10^5$
wild-type	1.4 ± 0.1	5.3 ± 0.2	3.6 ± 0.2
E64P	0.044 ± 0.002	1.0 ± 0.1	1.7 ± 0.1
E64G	0.043 ± 0.001	1.0 ± 0.1	2.0 ± 0.2
E64S	0.043 ± 0.002	1.0 ± 0.1	2.0 ± 0.1
N70V[a]	0.12, 0.03[b]	0.12	0.20[c]
N70D[a]	0.15	0.45	0.58[c]

[a] Reference 16. [b] Two phases were observed. [c] Calculated from the initial reaction rate under the steady-state condition, k_1 and k_2.

Table 6: Redox Potential (Fe^{2+}/Fe^{3+} Couple) of Wild-Type, E64P, E64G, and E64S HRPs

HRP	E_0/mV
wild-type	−261
E64P	−203
E64G	−213
E64S	−199
N70D[a]	−267

[a] Reference 18.

observed by ^{1}H NMR spectra of cyanide-ligated ferric low-spin forms of the mutants. One of the notable spectral features is the large upfield shift of N_ϵH in the distal His. Since the resonance position of the distal histidyl N_ϵH depends on the dipolar shift from the anisotoropic paramagnetic center of the heme iron (*45*), the deviation of the resonance position can be interpreted as the reorientation of the distal His (*18*). The reorientation of the distal His is also supported by the large downfield shift of C_ϵH in the proximal His. Although the proximal His is not directly connected to the distal His, the perturbation in the orientation of the distal His can be transmitted to the proximal His through the hydrogen bond between the distal His and heme-bound cyanide, affecting the hyperfine-shifted resonance of the proximal His C_ϵH (*46*, *47*). The large downfield shift of C_ϵH in the proximal His in the mutants, therefore, would correspond to the reorientation of the distal His.

As reported in our previous study, the reorientation of the distal His is implicated with disruption of the hydrogen bond between the distal His and Asn70 (*18*). The signal broadening for the distal His N_δH (16.6 ppm) in the ^{1}H NMR spectra (Figure 3) of the Glu64 mutants, which was also manifested in the spectrum of the N70D mutant (*18*), can be attributable to a fast chemical exchange of the N_δH in the distal His with protons of bulk water (*48*), indicating cleavage of the His−Asn hydrogen bond (*18*). The spectral similarity between the Glu64 mutants and the N70D mutant leads us to conclude that the disruption of the His−Asn hydrogen bond reoriented the distal His in the Glu64 mutants. The effect of the missing hydrogen bond between the distal His and Asn70 is prominent in the basicity of the distal His. The distal His has a hydrogen bond with the adjacent Asn residue, which is a common feature in peroxidase and promotes the peroxidase reaction by raising the basicity of the distal His. In fact, the pH-dependent Raman frequency shifts of the iron−histidine stretching band suggested the lower basicity of the distal His in the Asn70 mutants, in which the His−Asn hydrogen bond is cleaved (*17*). Although the pH dependence of the stretching bond in the Glu64 mutants has not yet been examined due to the small expression level of the mutant proteins, the basicity of the distal His in the Glu64 mutant would be also decreased due to the breakage of the His−Asn hydrogen bond.

Such perturbations in the distal site were also detected around the distal Arg, which is one of the most conserved and key residues for peroxidase activity. As evidenced by the ^{1}H NMR spectra of the cyanide-ligated forms, the resonance positions for C_βH and C_δH of the distal Arg were affected by the mutation at Glu64 (see Results), indicating the positional change of the distal Arg in the Glu64 mutants. Thus, the perturbation of the distal Arg is responsible for the disruption of the hydrogen bond between the ferryl oxygen and the N_ϵH of the distal Arg in the mutant compounds II, which was found by the increase of the Fe^{IV}═O stretching Raman frequency (Figure 5).

In addition to the structural defects on the distal side, ICP emission spectroscopy found the loss of one calcium ion in all the Glu64 mutants. Recently, it was shown that a single mutation at the amino acid residue coordinating to a distal calcium ion can dissociate the calcium ion in manganese peroxidase (MnP) (*49*). In the present study, the absence of the carboxylate at position 64 interacting with the distal calcium ion through a water molecule would be enough to dissociate the distal calcium ion,[6] indicating that the carboxylate in the side chain of Glu64 is crucial for tethering the distal calcium ion. The X-ray crystal structure of MnP showed that the distal calcium ion structurally maintains amino acid residues above the heme in helix B, including the distal His and Arg (*11*). Upon the loss of the distal calcium ion, the distal His ligated to the heme iron to form a six-coordinated heme and the peroxidase activity was suppressed, implying that the dissociation of the distal calcium ion rearranged the distal amino acid residues essential for peroxidase activity in MnP. In the HRP Glu64 mutants, it is likely that the loss of the distal calcium ion induced distinct changes in the heme environment of the enzyme as well as the catalytic activity. As the ^{1}H NMR spectra in cyanide-ligated forms has revealed, the disruption of the His−Asn hydrogen bond, the reorientation of the distal His, and the positional change of the distal Arg in the distal cavities of the mutants were induced by the mutation at Glu64, which depressed the peroxidase activity, although it has not been clear whether these functional and structural

[6] The oxidation activities for hydroquinone of the mutants (2 μM) were not significantly enhanced by addition of excess calcium ion (5 mM) (data not shown). This result shows that a calcium ion fails to bind to the distal sites of the mutants in the presence of excess amount of calcium ion, suggesting the large dissociation constant of the distal calcium ion.

defects are attributable to the dissociation of the distal calcium ion or the cleavage of the hydrogen bond between Glu64 and Asn70. One of the key results is the close similarity of the catalytic and spectral properties of the E64S mutant to those of the E64P and E64G mutants. As shown in some mutagenetic studies (*50*−*53*), an amino acid replacement by proline or glycine residue often seriously perturbs the configuration of the main chain, whereas the structural effects would be much smaller in the replacement by serine residue. Thus, the deviations in the main chain for the serine (E64S) mutant would be much less than those for the proline (E64P) and glycine (E64G) mutants, which exhibited the functional and structural defects. However, the catalytic and spectral properties of the serine mutant were quite similar to those of the other mutants, suggesting that the rearrangements of the distal cavity in all the Glu64 mutants were caused by the dissociation of the distal calcium ion rather than by the disruption of the hydrogen bond between Glu64 and Asn70. In the present stage, we cannot rule out the possibility that configuration of the carbonyl oxygen on the main chain in the E64S mutant is also perturbed as expected for the E64P and E64G mutants. Crystallographic studies are now in progress to investigate the structural rearrangements in the distal cavities of the Glu64 mutants in more detail.

Our current results also shed light on the roles of the calcium ion in the proximal site. While the previous NMR study revealed that the removal of two calcium ions from native HRP caused large upfield shifts of the resonances for heme peripheral methyl groups and the proximal histidyl $N_\delta H$ in the ^1H NMR spectrum of the ferric state (*22*), the deviations of the resonance positions in the Glu64 mutants from those in wild-type enzyme were rather small. Although the dispersion of the resonance from the heme methyl groups in the ferric mutants was different from that in wild-type enzyme as shown in Figure 2, the average position for the four methyl group was insensitive to the mutation. In addition, the resonance position of the proximal His $N_\delta H$ in the mutants lacking the distal calcium ion appeared around 101 ppm, which coincided well with that in the parent enzyme. These spectral similarities suggest little perturbation around the proximal His in the Glu64 mutants.[7] Thus, elimination of the proximal calcium ion is expected to induce the remarkable shifts in the hyperfine-shifted resonances of the heme peripheral methyl groups and the proximal His $N_\delta H$ as found for the calcium-free native HRP (*22*), suggesting that the proximal calcium ion retains the geometry of the heme and the coordination structure of the proximal His.

Peroxidase Activities. The oxidation activity for ABTS was enhanced by the replacement of Glu64 in contrast to that for hydroquinone (Table 4). The rearrangement in the distal site of the mutants indicated by the NMR spectra would be a primary factor affecting the ABTS activity. However, as previous studies have shown, such perturbations depressed the activity but never enhanced it (*28*, *54*, *55*). It is thus unlikely that the enhancement of the ABTS activity is due to the rearrangement in the distal cavity. Instead, our and other groups have demonstrated that the higher reduction potential of compound II in the HRP Asn70 mutants (*16*) and *Arthromyces ramosus* peroxidase (ARP) (*27*) increases the ABTS activity. The increase of the reduction potentials for compounds II of the Glu64 mutants were also supported by Figure 7b. The more ready reduction of compound II to the resting state in the mutants than that in the wild-type enzyme shows destabilization of the mutant compounds II, which corresponds to the high reduction potential of compound II. Similar time-dependent UV−visible spectra were observed for the HRP Asn70 mutants and ARP having high reduction potentials of compounds II (*15*, *16*, *27*). Thus, the improvement of ABTS activity in the Glu64 mutants would be responsible for the higher reduction potentials of their compounds II. However, peroxidase activity for hydroquinone was highly retarded by the mutation at the Glu64, which cannot be explained by the increase of the reduction potential of compound II. The oxidation reaction of hydroquinone is quite different from that of ABTS, in that it requires a proton abstraction. In the initial step in the reduction of compound II, abstraction of a proton from hydroquinone would be substantially decelerated probably due to absence of the hydrogen bond between the ferryl oxygen and the distal Arg. To confirm the deceleration in the proton abstraction process and discuss the effects of the mutation on the peroxidase activity in more detail, we examined the elementary reaction rates (k_1, k_2, and k_3) in the catalytic cycle.

The formation rate of compound I (k_1) depends on the catalytic reactivity of the distal His as a general acid−base catalyst. The distal His is considered to facilitate the formation of the initial Fe−OOH complex (compound 0) by deprotonating a H_2O_2 as a base and subsequently assists the heterolytic cleavage of the O−O bond by protonating the distal oxygen as an acid (*3*−*5*). The disruption of the hydrogen bond by the mutation at Asn70 hydrogen-bonded with the distal His caused the reorientation and decrease of the basicity of the distal His, resulting in deceleration of k_1 to less than 10% of the wild-type enzyme (*15*−*18*). The His−Asn hydrogen bond is essential for the rapid reaction with H_2O_2 by controlling the position and basicity of the distal His (*15*−*18*, *54*, *56*, *57*). As observed in the previous studies, the reorientation of the distal His and decreased basicity by the rearrangement of the distal cavity would result in the depression of the k_1 values in the Glu64 mutants. The alternative amino acid residue responsible for the high reactivity toward H_2O_2 is Arg38. The distal Arg stabilizes the negative charge that develops in the transition state during the cleavage of the O−O bond in the iron−peroxide complex (*3*, *58*), which also facilitates the scission of the O−O bond. As indicated by ^1H NMR spectra, the position of the distal Arg is perturbed by the mutation, suggesting that the positional change of the distal Arg also decelerates the reaction rate with H_2O_2.

Another factor to decrease the k_1 values for the mutants would be the redox potentials of the Fe^{2+}/Fe^{3+} couple. The redox potentials of the Fe^{2+}/Fe^{3+} couple of the Glu64 mutants are increased by ∼60 mV, compared with that of the wild-

[7] We observed the large deviations of the signal position for the proximal His $C_\epsilon H$ in the cyanide-bound mutants from those in the wild-type enzyme (Figure 3). However, the chemical shift of the resonance in the cyanide-bound form highly depends on the configuration of the liganded cyanide in addition to the structural alterations on the proximal side (*46*, *47*). Since the configuration of the liganded cyanide would be affected by the cleavage of the hydrogen bond with the distal His in the mutants, it is unlikely that the spectral changes of the mutants in Figure 3 arise from the large structural changes in the proximal site.

type enzyme.[8] The higher redox potential of the Fe^{2+}/Fe^{3+} couple is considered to decelerate the cleavage rate of the O−O bond in the peroxide-bound iron complex (*62*), resulting in decrease of the formation rate of compound I. For instance, k_1 of a CcP D235N mutant was decreased ∼5-fold presumably due to the increase of its redox potential (Fe^{2+}/Fe^{3+}) by ∼100 mV (*4*, *61*). Therefore, the increase of the redox potential (Fe^{2+}/Fe^{3+}) as well as the reorientation and reduced basicity of the distal His might be responsible for the greater decrease of the k_1 values observed in the Glu64 mutants.[9]

The reduction rates of the mutants' compounds I (k_2) also decreased to 20% of the parent enzyme. The reduction of compound I is accomplished by uptake of a proton from the substrate and the subsequent electron transfer from the substrate to porphyrin moiety (*65*). We previously reported that less basicity and improper orientation of the distal residue impaired the uptake of a proton from the substrate (*16*, *18*, *57*). In the Glu64 mutants, the perturbation of the distal His would retard the abstraction of a proton from substrates, resulting in the decreased k_2.

The reduction rates of mutant compounds II (k_3) decreased 2-fold, relative to that of wild-type enzyme. One of the factors to control the k_3 step is the reduction potential of compound II (*66*). The higher oxidation activity for ABTS strongly suggests that the reduction potential of compound II is increased in the Glu64 mutants. The high reduction potential of compound II leads to the acceleration of the k_3 process. However, it is not the case for the Glu64 mutants, since the k_3 process was decelerated in the mutants. A hydrogen bond between a ferryl oxygen in compound II and $N_\epsilon H$ in the distal Arg would be another key factor to determine the k_3 value (*37*, *39*, *40*). In the present study, the Fe^{IV}═O Raman band in the mutant compounds II at pD 7.0 appeared at the position of wild-type HRP at pD 10.0 where the ferryl oxygen−Arg hydrogen bond is disrupted. This observation clearly indicates that the hydrogen bond is not formed in the Glu64 mutants at neutral pH, due to the positional change of the distal Arg. Since the disruption of the hydrogen bond markedly depresses the reaction rate of compound II (*37*, *39*, *40*), the acceleration effects of the reduction potential on the reaction rate would be canceled out.

In summary, the E64P and E64G mutants showed substantially depressed oxidation activities for hydroquinone and elementary reaction rates in the catalytic cycle. ^{1}H NMR spectra revealed the disruption of the His−Asn hydrogen bond and the reorientation of the distal His in the mutants. However, the E64S mutant, which is supposed to have the same configuration of the carbonyl oxygen on the main chain as the wild-type enzyme, also exhibited catalytic and spectral properties quite similar to those of the E64P and E64G mutants. The catalytic and structural defects observed in the three mutants were found to be due to dissociation of the distal calcium ion by removal of the carboxylate in the side chain of the Glu64 residue rather than the disruption of the hydrogen bond between Glu64 and Asn70. These results lead us to conclude that the Glu64 residue, one of the amino acid residues forming the hydrogen bond network in the distal site, is crucial for stable binding of the distal calcium ion, which maintains the structural integrity of the distal cavity, resulting in high catalytic activities.

[8] Previous works on C*c*P mutants have shown that the increase of the redox potential for the Fe^{2+}/Fe^{3+} couple arises from changes in the conserved interactions between the proximal His and a neighboring Asp residue (*59*−*61*). In this study, however, perturbation was not found around the proximal His in the Glu64 mutants. Therefore, it is likely that the increase of the redox potential for the Fe^{2+}/Fe^{3+} couple observed in the Glu64 mutants was due to the structural rearrangement in the distal cavity.

[9] Although the midpoint potential for the Fe^{2+}/Fe^{3+} couple in C*c*P (−194 mV) (*63*) is approximately equal to the HRP mutants described here (∼−200 mV), the reaction with hydrogen peroxide goes at faster rates in the C*c*P (3.4×10^7 $M^{-1}\cdot s^{-1}$) (*64*) than those in the HRP Glu64 mutants (4.3×10^5 $M^{-1}\cdot s^{-1}$). The relation between the midpoint potential and the reaction rate has not yet been clarified for comparison of HRP and C*c*P.

ACKNOWLEDGMENT

We are obliged to Prof. Teizo Kitagawa (Institute for Molecular Science) for the resonance Raman experiments. We are also grateful to Dr. Satoshi Takahashi (Kyoto University) for technical assistance with the resonance Raman experiments. We thank Prof. Shigeo Umetani (Kyoto University) for help with the ICP emission experiments. M.T. is supported by Research Fellowships of the Japan Society for the Promotion of Science for Young Scientists.

NOTE ADDED IN PROOF

Since the submission of this paper, the crystal structure of recombinant HRP-C has been published (*67*).

REFERENCES

1. Dolphin, D., Forman, A., Borg, D. C., Fajer, J., and Felton, R. H. (1971) *Proc. Natl. Acad. Sci. U.S.A. 68*, 614−618.
2. Schuller, D. J., Ban, N., van Huystee, R. B., McPherson, A., and Poulos, T. L. (1996) *Structure 4*, 311−321.
3. Poulos, T. L., and Kraut, J. (1980) *J. Biol. Chem. 255*, 8199−8205.
4. Erman, J. E., Vitello, L. B., Miller, M. A., and Kraut, J. (1992) *J. Am. Chem. Soc. 114*, 6592−6593.
5. Erman, J. E., Vitello, L. B., Miller, M. A., Shaw, A., Brown, K. A., and Kraut, J. (1993) *Biochemistry 32*, 9798−9806.
6. Newmyer, S. L., and Ortiz de Montellano, P. R. (1995) *J. Biol. Chem. 270*, 19430−19438.
7. Rodriguez-Lopez, J. N., Smith, A. T., and Thorneley, R. N. F. (1996) *J. Bioinorg. Chem.* 1, 136−142.
8. Finzel, B. C., Poulos, T. L., and Kraut, J. (1984) *J. Biol. Chem. 259*, 13027−13036.
9. Poulos, T. L., Edwards, S. L., Wariishi, H., and Gold, M. G. (1993) *J. Biol. Chem. 268*, 4429−4440.
10. Edwards, S. L., Raag, R., Wariishi, H., Gold, M. H., and Poulos, T. L. (1993) *Proc. Natl. Acad. Sci. U.S.A. 90*, 750−754.
11. Sundaramoorthy, M., Kishi, K., Gold, M. H., and Poulos, T. L. (1994) *J. Biol. Chem. 269*, 32759−32767.
12. Kunishima, N., Fukuyama, K., Matsubara, H., Hatanaka, H., Shibano, Y., and Amachi, T. (1994) *J. Mol. Biol. 235*, 331−344.
13. Petersen, J. F. W., Kadziola, A., and Larsen, S. (1994) *FEBS Lett. 339*, 291−296.
14. Patterson, W. R., and Poulos, T. L. (1995) *Biochemistry 34*, 4331−4341.
15. Nagano, S., Tanaka, M., Watanabe, Y., and Morishima, I. (1995) *Biochem. Biophys. Res. Commun. 207*, 417−423.
16. Nagano, S., Tanaka, M., Ishimori, K., Watanabe, Y., and Morishima, I. (1996) *Biochemistry 35*, 14251−14258.
17. Mukai, M., Nagano, S., Tanaka, M., Ishimori, K., Morishima, I., Ogura, T., Watanabe, Y., and Kitagawa, T. (1997) *J. Am. Chem. Soc. 119*, 1758−1766.

18. Tanaka, M., Nagano, S., Ishimori, K., and Morishima, I. (1997) *Biochemistry 36*, 9791−9798.
19. Smith, A. T., Santama, N., Dacey, S., Edwards, M., Bray, R. C., Thorneley, R. N. F., and Burke, J. F. (1990) *J. Biol. Chem. 265*, 13335−13343.
20. Haschke, R. H., and Friedhoff, J. M. (1978) *Biochem. Biophys. Res. Commun. 80*, 1039−1042.
21. Ogawa, S., Shiro, Y., and Morishima, I. (1979) *Biochem. Biophys. Res. Commun. 90*, 674−678.
22. Shiro, Y., Kurono, M., and Morishima, I. (1986) *J. Biol. Chem. 261*, 9382−9390.
23. Morishima, I., Kurono, M., and Shiro, Y. (1986) *J. Biol. Chem. 261*, 9391−9399.
24. Paul, K. G., Theorell, H., and Akesson, A. (1953) *Acta Chem. Scand. 7*, 1284−1287.
25. Chen, Y. H., Yang, J. T., and Martinez, H. M. (1972) *Biochemistry 11*, 4120−4131.
26. Sawaki, Y., and Foote, C. S. (1979) *J. Am. Chem. Soc. 101*, 6292−6296.
27. Farhangrazi, Z. S., Copeland, B. R., Nakayama, T., Amachi, T., Yamazaki, I., and Powers, L. S. (1994) *Biochemistry 33*, 5647−5652.
28. Smith, A. T., Sanders, S. A., Thorneley, R. N. F., Burke, J. F., and Bray, R. C. (1992) *Eur. J. Biochem. 207*, 507−519.
29. Yamada, H., Makino, R., and Yamazaki, I. (1975) *Arch. Biochem. Biophys. 169*, 344−353.
30. Clark, W. M. (1960) *Oxidation−Reduction Potentials of Organic Systems*, Williams & Wilkins Co., Baltimore, MD.
31. Strickland, E. H. (1968) *Biochim. Biophys. Acta 151*, 70−75.
32. La Mar, G. N., de Ropp, J. S., Smith, K. M., and Langry, K. C. (1980) *J. Biol. Chem. 255*, 6646−6652.
33. Veitch, N. C., Williams, R. J. P., Bray, R. C., Burke, J. F., Sanders, S. A., Thorneley, R. N. F., and Smith, A. T. (1992) *Eur. J. Biochem. 207*, 521−531.
34. de Ropp, J. S., Mandal, P., Brauer, S. L., and La Mar, G. N. (1997) *J. Am. Chem. Soc. 119*, 4732−4739.
35. Thanabal, V., de Ropp, J. S., and La Mar, G. N. (1987) *J. Am. Chem. Soc. 109*, 7516−7525.
36. Satterlee, J. D., Alam, S. L., Mauro, J. M., Erman, J. E., and Poulos, T. L. (1994) *Eur. J. Biochem. 224*, 81−87.
37. Sitter, A. J., Reczek, C. M., and Terner, J. (1985) *J. Biol. Chem. 260*, 7515−7520.
38. Fülöp, V., Phizackerley, P. R., Soltis, S. M., Clifton, I. J., Wakatsuki, S., Erman, J., Hajdu, J., and Edwards, S. L. (1994) *Structure 3*, 201−208.
39. Makino, R., Uno, T., Nishimura, Y., Iizuka, T., Tsuboi, M., and Ishimura, Y. (1986) *J. Biol. Chem. 261*, 8376−8382.
40. Hashimoto, S., Tatsuno, Y., and Kitagawa, T. (1986) *Proc. Natl. Acad. Sci. U.S.A. 83*, 2417−2421.
41. Teraoka, J., and Kitagawa, T. (1981) *J. Biol. Chem. 256*, 3969−3977.
42. Kitagawa, T., Nagai, K., and Tsubaki, M. (1979) *FEBS Lett. 104*, 376−378.
43. Yamazaki, I., and Yokota, K. (1973) *Mol. Cell. Biochem. 2*, 39−52.
44. Critchlow, J. E., and Dunford, H. B. (1972) *J. Biol. Chem. 247*, 3703−3713.
45. Sheard, Y., Yamane, T., and Shulman, R. G., (1970) *J. Mol. Biol. 63*, 35−48.
46. Emerson, S. D., and La Mar, G. N. (1990) *Biochemistry 29*, 1556−1566.
47. La Mar, G. N., Chen, Z., Vyas, K., and McPherson, A. D. (1995) *J. Am. Chem. Soc. 117*, 411−419.
48. Thanabal, V., de Ropp, J. S., and La Mar, G. N. (1988) *J. Am. Chem. Soc. 110*, 3027−3035.
49. Sutherland, G. R. J., Zapanta, L. S., Tien, M., and Aust, S. D. (1997) *Biochemistry 36*, 3654−3662.
50. Matthews, B. W., Nicholson, H., and Becktel, W. J. (1987) *Proc. Natl. Acad. Sci. U.S.A. 84*, 6663−6667.
51. Alber, T., Dao-pin, S., Wilson, K., Wozniak, J. A., Cook, S. P., and Matthews, B. W. (1987) *Nature 330*, 41−46.
52. Alber, T., Bell, J. A., Dao-pin, S., Nicholson, H., Wozniak, J. A., Cook, S. P., and Matthews, B. W. (1988) *Science 239*, 631−635.
53. Yutani, K., Hayashi, S., Sugisaki, Y., and Ogasahara, K. (1991) *Proteins 9*, 90−98.
54. Savenkova, M. I., Newmyer, S. L., and Ortiz de Montellano, P. R. (1996) *J. Biol. Chem. 271*, 24598−24603.
55. Gazaryan, I. G., Doseeva, V. V., Galkin, A. G., and Tishkov, V. I. (1994) *FEBS Lett. 354*, 248−250.
56. Tanaka, M., Ishimori, K., and Morishima, I. (1996) *Biochem. Biophys. Res. Commun. 227*, 393−399.
57. Tanaka, M., Ishimori, K., Mukai, M., Kitagawa, T., and Morishima, I. (1997) *Biochemistry 36*, 9889−9898.
58. Vitello, L. B., Erman, J. E., Miller, M. A., Wang, J., and Kraut, J. (1993) *Biochemistry 32*, 9807−9818.
59. Fishel, L. A., Villafranca, J. E., Mauro, J. M., and Kraut, J. (1987) *Biochemistry 26*, 351−360.
60. Vitello, L. B., Erman, J. E., Miller, M. A., and Kraut, J. (1992) *Biochemistry 31*, 11524−11535.
61. Goodin, D. B., and McRee, D. E. (1993) *Biochemistry 32*, 3313−3324.
62. Dawson, J. H., and Sono, M. (1987) *Chem. Rev. 87*, 1255−1276.
63. Conroy, C. W., Tyma, P., Daum, P. H., and Erman, J. E. (1978) *Biochim. Biophys. Acta 537*, 62−69.
64. Ohlsson, P. I., Yonetani, T., and Wold, S. (1986) *Biochim. Biophys. Acta 874*, 160−166.
65. Dunford, H. B. (1991) in *Peroxidases in Chemistry and Biology* (Everse, J. E., Everse, K. E., and Grisham, M. B., Eds.) Vol. II, pp 1−24, CRC Press, Boca Raton, FL.
66. Hayashi, Y., and Yamazaki, I. (1979) *J. Biol. Chem. 254*, 9101−9106.
67. Gajhede, M., Schuller, D. J., Henriksen, A., Smith, A. T., and Poulos, T. L. (1997) *Nat. Struct. Biol. 4*, 1032−1038.

BI9725273